Considering the saturation effect in nuclei based on the Kharzeev-Levin-Nardi model

F. Muhammadi* and B. Rezaei†
Department of Physics, Razi University, Kermanshah 67149, Iran

(Received 25 June 2022; accepted 26 July 2022; published 22 August 2022)

We consider the total and longitudinal cross sections by using the color dipole model according to the known Kharzeev-Levin-Nardi model in nuclei. Our calculations can predict the low-x electron-nucleus cross sections, the saturation effect, and the ratio between the structure functions for different nuclei and energies of colliding particles. The results indicate the differences between two perturbative and nonperturbative regions at low x, which are compared with the H1, ZEUS, New Muon, and E665 Collaborations.

DOI: 10.1103/PhysRevC.106.025203

I. INTRODUCTION

It is well-known that the study of cross sections and structure functions in high-energy interaction between an electron and a proton or nuclei provides a new understanding of the low-x region of quantum chromodynamics (QCD). Although QCD of the low-x nuclear interactions have various similarities with light particle collisions, some new physics exist in the former. It has been a long time since the nuclear parton distribution functions (nPDFs) and structure functions have been studied [1,2], but our understanding of them is still incomplete. Therefore, to uncover the secrets of nuclear matter we need a proper theoretical prediction and new experimental data to verify them. In this way, the future Electron-Ion Collider (EIC) at Brookhaven National Laboratory [3,4] and the Large Hadron Electron Collider (LHeC) at CERN [5] will provide a good opportunity to unravel the mystery surrounding nuclear structure function. The difference between two perturbative and nonperturbative QCD regions, shadowing, and the saturation effect in small x can be studied with the help of new data.

In the low-x region of the high-energy QCD, the Balitsky-Fadin-Kuraev-Lipatov (BFKL) [6–8] equation or its improved forms, like the Gribov-Leven-Ryskin (GLR) [9] and the Balitsky-Kovchegov (BK) [10,11] equations, can be used to investigate the gluon distribution evolution.

The result of using the BFKL linear evolution is a significant rise in gluon numbers in small-x dynamics because of the ladder evolution of $g \to gg$. It leads to $\sigma_{\rm tot} \approx s^{\alpha_P - 1}$ and the power $\alpha_P - 1 > 0$ for which the cross section would violate the Froissart bound. The Froissart-bound limits $\sigma_{\rm tot}$ to be smaller than $\ln^2 s$.

A modified version of the BFKL equation is the nonlinear GLR equation, which tackles the BFKL unitarity problem by subtracting a new quadratic term of the gluon distribution. This nonlinear term causes the recombination of gluons, $gg \to g$, which slows down the growth of the gluon numbers in small-x and high-Q^2 values. This phenomenon is known as the saturation effect [12]. It adapts $\sigma_{\rm tot}$ to the Froissart-bound. The perturbation method is valid when the strong coupling, as the function of a definite scale, takes small values [13]. In the high-energy region of the QCD, Q_s is a proper scale that provides this condition and determines the critical line that separates the linear region from the saturation region. If we assume $\mathbf{k_T}$ as the transverse momentum of the gluon, the transverse size of the gluon $\approx 1/k_T$. Gluon fusions $gg \to g$ occur at large transverse sizes (*small* $\mathbf{k_T}$); in this way the saturation effect is weak for $\mathbf{k_T^2} > Q_s^2$ and strong for $\mathbf{k_T^2} < Q_s^2$. We want to show these differences in nuclear cross sections, structure functions, and their ratio. Several other attempts have been made to generalize the equations by Ayala–Gay Ducati–Levin [14], Balitsky, and Kovchegov.

The Kharzeev-Levin-Nardi (KLN) model [15] as a phenomenologically tested model [16–18] represents the gluon distribution of the proton which involves saturation, linear, and nonlinear physics. In this paper, we generalize this model to *nuclear targets* with the appropriate saturation scale for nuclei and we combine the results with the color dipole model (CDM) to calculate cross sections.

The CDM is a strong approach developed by Nikolaev and Zakharov [21] to analyze inclusive or diffractive[1] processes and their cross sections in deep inelastic scattering (DIS). In this approach, a (virtual) photon is scattered off a fixed-target hadron in such a way that the latter will carry more energy. The photon has enough energy to fluctuate into a pair of $q\bar{q}$ (a dipole). So we can consider the dipole-hadron interaction instead of the main photon-hadron process. Since the formation time of the $q\bar{q}$ pair is longer than the interaction time, the transverse size of the dipole is approximately frozen during the interaction with the target. This picture factorizes the main process (γ^*-target) cross section into the (virtual) photon-pair wave function and dipole cross section. The factorization

*f.muhammadi@razi.ac.ir
†brezaei@razi.ac.ir

[1]In Refs. [19,20], the authors review diffractive processes.

capability makes this viewpoint very strong and popular. Another way to study the γ^*-target process is to consider γ^*–sea quark interactions [22–24].

Golec-Biernat and Wüsthoff [25] have introduced a famous model for the dipole cross section. This model has attracted great attention not just for how it treated the problem but for the recognition of geometric scaling [25,26]. One of the perfect predictions of color glass condensate (CGC) [27–29] and saturation physics [30] is the agreement between experimental data and the geometric scaling property [31–35] of total DIS cross sections, which states that the total cross section only depends on the *geometric scaling variable* $\tau = {Q^2}/{Q_s^2}$.

Recently, some other models have been proposed for dipole cross sections [36–40]. Mostly, by using a forward scattering amplitude and the eikonal approximation [41,42], they have calculated the dipole cross section. The IP-SAT [37] and b-CGC [36] models have succeeded in illustrating the data for dipole-proton interaction very well, and an interesting comparison between these two ideas can be found in Ref. [43].

Fixed-target DIS experimental data show that the ratio (R) of the structure function per nucleon for a nucleus (${F_2^A}/{A}$) to a nucleon structure function (${F_2^D}/{2}$) does not equal unity for various x [44,45]. The reason for using a deuteron is to contain the nearest approximation to the structure of a single nucleon. This observable, which is a proper quantity to examine nuclear effects on QCD, requires a multilateral study.

The paper is organized as follows. Section II gives a review of the CDM, then KLN model, and the calculations of the dipole cross section. In Sec. III, we present the results, the diagrams, and a comparative study that includes nuclear cross sections, structure functions, and the R ratio. Finally, our conclusions are given in Sec. IV.

II. APPLYING THE KLN MODEL IN THE DIPOLE FRAME

In the small-x region, the nuclear structure functions F_2^A and $F_{\rm L}^A$ can be defined for transverse (T) or longitudinal (L) photons via the cross sections $\sigma_{\rm T,L}^A$:

$$F_2^A = \frac{Q^2}{4\pi^2\alpha}\,\sigma_{\rm tot}^A = \frac{Q^2}{4\pi^2\alpha}\left(\sigma_{\rm T}^A + \sigma_{\rm L}^A\right), \tag{1}$$

$$F_{\rm L}^A = \frac{Q^2}{4\pi^2\alpha}\sigma_{\rm L}^A. \tag{2}$$

The dipole picture belongs to s-channel models. It is formulated in impact parameter space [46]. This picture is an alternative approach to investigate low-x DIS and, as mentioned earlier, it includes two main subprocesses: First, the virtual photon fluctuates in a quark-antiquark pair (dipole) and then the latter interacts with the nucleus.

In this picture, the known expression for DIS cross sections reads as follows [47]:

$$\sigma_{\rm T,L}^{\gamma^* P} = \int_0^1 dz \int d^2r |\Psi_{\rm L,T}(z,r)|^2 \sigma(x,r^2). \tag{3}$$

Q^2, z, and $1-z$ are the photon virtuality and the fraction of the longitudinal momentum carried by the quark and the antiquark in the light cone frame, respectively. $\Psi_{\rm L,T}$ are photon wave functions calculable in perturbation theory:

$$|\Psi_{\rm L,T}|^2 = \frac{6\alpha}{4\pi^2}\sum_q e_q^2 \times \begin{cases} [z^2+(1-z)^2]\varepsilon^2 K_1^2(\varepsilon r) + m_q^2 K_0^2(\varepsilon r) & \text{(T)}, \\ 4Q^2 z^2 (1-z)^2 K_0^2(\varepsilon r) & \text{(L)}, \end{cases} \tag{4}$$

where $\varepsilon^2 = z(1-z)Q^2 + m_q^2$. The dominant contribution in Eq. (4) is obtained for $\varepsilon r < 1$ in which limit, McDonald functions $K_0(\varepsilon r) \approx \theta(1-\varepsilon r)$ and $K_1(\varepsilon r) \approx {\theta(1-\varepsilon r)}/{\varepsilon r}$ with the Heaviside step function θ. Summation is performed over quark flavors, with the charge e_q and the mass m_q.

The *dipole cross section* $\sigma(x,r^2)$ is the total cross section of the interaction between the $q\bar{q}$ pair and the target. This quantity, which includes the nonlinear effects of interaction, is a function of relative transverse pair separation r and x ($x = x_{Bj}$ for light quarks and $x = x_{Bj}(1 + m_Q^2/Q^2)$ for heavy quarks [48]). The dipole cross section can be calculated by having a gluon distribution function [49]:

$$\sigma(x,r^2) \approx \frac{\pi^2}{3} r^2 \alpha_s(r) x g\left(x, \frac{1}{r^2}\right). \tag{5}$$

Kharzeev, Levin, and Nardi proposed a simple saturation model [15] by considering the *cross section of the probe partons* ($\sigma \approx \alpha_s/Q^2$) and the *density of partons* ($\rho_A \approx {x g_A(x,Q^2)}/{\pi R_A^2}$) in a transverse plane in which the hard probe interacts with the nucleus within the target area. Two regimes, $\sigma\rho_A \ll 1$ and $\sigma\rho_A \gg 1$, describe a dilute parton system and a dense parton system, respectively, and $\sigma\rho_A \approx 1$ determines the critical line that discriminates between linear and nonlinear regions at the saturation scale of $Q = Q_s$:

$$\frac{\alpha_s}{Q_s^2}\frac{x g_A\left(x, Q_s^2\right)}{\pi R_A^2} \approx 1. \tag{6}$$

In this way, the KLN form of the gluon distribution function is

$$x g_p\left(x, p_t^2\right) = \begin{cases} \frac{\kappa_0}{\alpha_s(Q_s^2)} S p_t^2 (1-x)^4, & p_t \leqslant Q_s(x), \\ \frac{\kappa_0}{\alpha_s(Q_s^2)} S Q_s^2(x)(1-x)^4, & p_t > Q_s(x), \end{cases} \tag{7}$$

where $(1-x)^4$ factors ensure a low gluon density at the high-x values. The normalization coefficient κ_0 can be determined by comparing the results of substituting the KLN gluon distribution, Eq. (7), and different parametrizations of the gluon density like GRV98 [50] in the momentum sum rule condition. S is the area of the target. The running coupling α_s at the leading order approximation with the number of active quark flavors N_f and $\Lambda = 0.224$ GeV is

$$\alpha_s = \frac{4\pi}{\frac{1}{3}(33-2N_f)\ln\frac{Q^2}{\Lambda^2}} \tag{8}$$

and the saturation scale Q_s is given by [25,51]

$$Q_s^2 = Q_0^2\left(\frac{x_0}{x}\right)^{\lambda}, \tag{9}$$

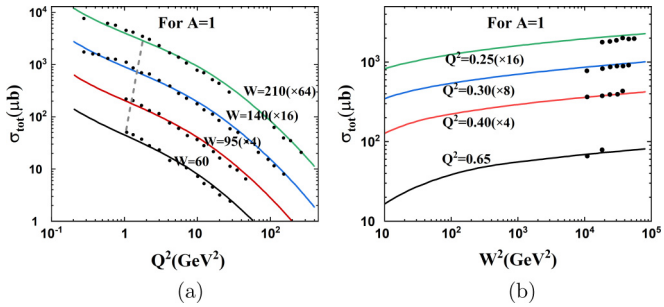

FIG. 1. Total proton cross sections as a function of Q^2 (a) for different W and (b) as a function of W^2 for different Q^2 based on our analysis. Solid points show H1 and ZEUS data. (a) $\sigma_{\rm tot}$ in Q^2 for different W (b) $\sigma_{\rm tot}$ in W^2 for different Q^2.

where x_0, Q_0, and λ are three constants that have been obtained from the experimental data and parameter fitting procedures for DIS of $\gamma^* p$.

The KLN model could be generalized to include different nuclei by substituting the photon virtuality Q^2 instead of p_t^2, $S \to S_A = A^{2/3}S$, $Q_s^2 \to Q_{s,A}^2 = A^{1/3}Q_s^2$, and $R_s^2 = \frac{1}{Q_s^2}$ in Eq. (7):

$$xg_A(x,Q^2) = \begin{cases} A\frac{\kappa_0}{\alpha_s(A^{1/3}Q_s^2)} S\,\frac{1}{R_s^2}(1-x)^4, & r^2 \leqslant \frac{R_s^2}{A^{1/3}}, \\ A^{2/3}\frac{\kappa_0}{\alpha_s(A^{1/3}Q_s^2)} S\,\frac{1}{r^2}(1-x)^4, & r^2 > \frac{R_s^2}{A^{1/3}}. \end{cases} \quad (10)$$

The reasons for these changes are the atomic mass dependency of the nuclear charge radius ($R \propto A^{1/3}$) and the relation between the saturation scale and the atomic mass ($Q_s^2 \propto A^{\frac{1}{3}}$).

So, the *nuclear dipole cross section* is obtained by inserting Eqs. (10) and (8) into Eq. (5) and making some simplifications:

$$\sigma^A(x,r^2) = \frac{\pi^2}{3}(\kappa_0 S)^{\rm proton}\,(1-x)^4 \times \begin{cases} A\frac{r^2}{R_s^2}\frac{\ln R_s^2\Lambda^2 - \ln A^{1/3}}{\ln \Lambda^2 r^2}, & r^2 \leqslant \frac{R_s^2}{A^{1/3}}, \\ A^{2/3}\frac{\ln R_s^2\Lambda^2 - \ln A^{1/3}}{\ln \Lambda^2 r^2}, & r^2 > \frac{R_s^2}{A^{1/3}}. \end{cases} \quad (11)$$

Equation (11) is a modified form of the KLN model that can be used to study the behavior of the dipole cross section in linear and nonlinear regions for different nuclei.

III. RESULTS

In the following, we present the nuclear cross sections, the structure functions, and the ratio R_{F_2} diagrams for the lightest nuclear target (hydrogen nucleus) and the heavier ones using Eqs. (1), (3), and (11). These quantities give us a real insight into the small-x behaviors of the nuclei. The nuclear target can be adjusted by setting the atomic mass number (A) in Eq. (11).

Figure 1 shows the total cross sections of a hydrogen nucleus by taking the average value of 0.14 GeV for the light quark masses. The lines are in agreement with H1 [52,53] and ZEUS [54] data [Figs. 1(a) and 1(b)].

In Fig. 1(a), the dashed oblique line shows the transition between linear and nonlinear regions in $Q^2 = Q_s^2$. The total $\gamma^* p$ cross section increases with decreasing Q^2 for definite

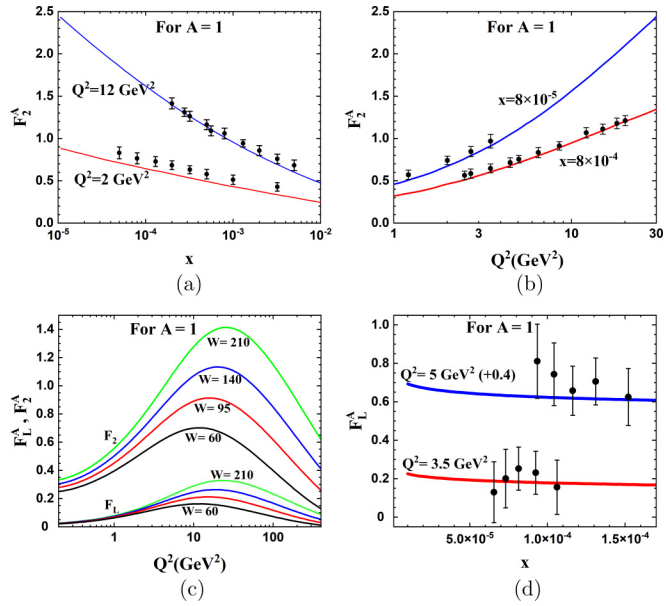

FIG. 2. Hydrogen target's structure functions based on our analysis. F_2 as a function of x (a) and Q^2 (b). F_2 and F_L vs Q^2 in a frame at different values of W (c) and F_L vs small x (d). Solid points show H1 and ZEUS data.

W. For the small transverse momentum of the gluon, gluon recombination causes the saturation effect to be visible as solid lines appear to reduce their slope by turning partly to a horizontal line in the small-Q^2 region. Our analysis is compatible with the experimental data in both regions. We expected to see linear and saturation differences because the foundation of Eq. (11) includes both of them. The factors 1, 4, 16, and 64 are just to make some separation between the lines in the small-Q^2 region.

In Fig. 1(b), we have shown the $\gamma^* p$ total cross section as a function of large W^2 at different values of $Q^2 = 0.65$, 0.40, 0.30, and 0.25 GeV^2 for which x is very small.

In Fig. 2, we have depicted the structure functions of F_2 and $F_{\rm L}$ for electron scattering off the hydrogen nucleus by using Eqs. (1) and (2). F_2 versus x and F_2 vs Q^2 are shown in Figs. 2(a) and 2(b), respectively. Fixed $Q^2 = 2$ and 12 GeV^2 and $x = 8 \times 10^{-4}$ and 8×10^{-5} are plotted there to investigate both small-x and low-Q^2 regions. Our calculated F_2 values reproduce the HERA data [55,56]. F_2 takes larger values in small x and increases with Q^2.

Figure 2(c) shows both F_2 and $F_{\rm L}$ together for $A = 1$ to make their comparison easier. According to our analysis, $F_{\rm L}$ accounts for 21% of F_2 in $Q^2 = 14$ GeV^2 and $x \approx 10^{-4}$, which is near 19% of HERA data as reported in Refs. [56,57].

In Fig. 2(d), $F_{\rm L}$ versus x is specially drawn for the low-x region and low values of Q^2. Experimental data with error bars are from H1 data [58].

Now, let us discuss the electron scattering of heavier nuclei. Deuteron, carbon, calcium, iron, tin, xenon, and lead are frequently used as nuclear targets in accelerators. We should consider that the experimental data for high-energy electron-nuclei collision in the small-x region is usually proposed as "R_{F_2} data" [59–65]. We use the existing data in different

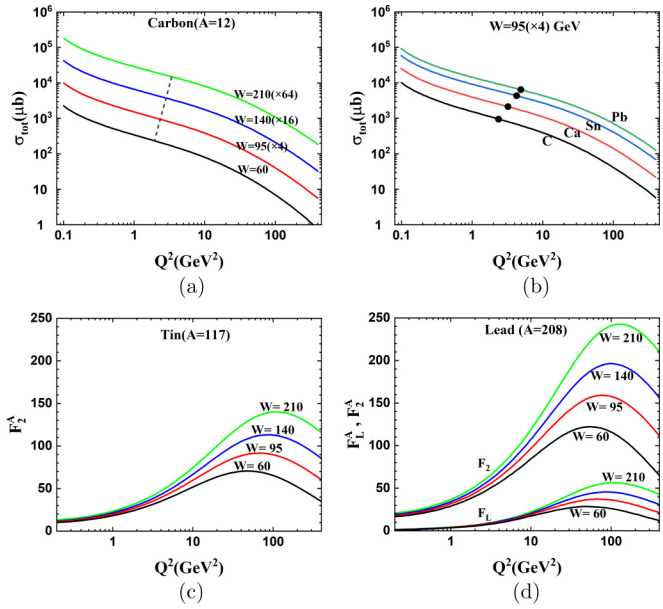

FIG. 3. $\sigma_{\rm tot}$ versus Q^2 for different energies and atomic masses of targets [panels (a) and (b)]. F_2 versus Q^2 for Sn and Pb nuclei [panels (c) and (d)] and lead's $F_{\rm L}$ as calculated in our analysis [panel (d)].

graphs for comparison. Also, we present some predictions about cross sections and structure functions for heavier nuclei in the saturation region and the low-x region.

In Fig. 3, the total cross sections and the structure functions are depicted for heavier nuclei. We see that for a certain target and definite Q^2, the nuclear cross section is increased by taking a larger value of W energy. The dashed oblique line in Fig. 3(a) shows the critical line ($Q = Q_s$). Besides this, the following two results are attained by looking at Fig. 3(b) drawn for fixed $W = 95$ GeV. First, heavier nuclei have larger cross sections for fixed Q and W. Second, transitions of the linear region to the saturation region, shown as solid points, are shifted to higher values of Q^2 for heavier nuclei.

Figures 3(c) and 3(d) illustrate the Q^2 dependence of F_2^A for nuclear targets of Sn and Pb. F_2^A is increased by taking larger values of W and A. F_L^A is calculated in Fig. 3(d), which accounts for 23% of F_2 for different energies of W in $Q^2 = 50$ GeV^2 for the lead nucleus.

According to Fig. 3, applying the heavier nuclei as targets can separate linear and nonlinear regions more explicitly even at larger Q^2 values. This important property is an excellent motivation to study the saturation physics for heavier nuclei in future accelerators.

Now, we compare our calculated R_{F_2} in electron-nuclei collisions with the results of New Muon Collaboration (NMC) experiments at CERN [59–63] and E665 Collaboration experiments at FermiLab [64,65]. Carbon and deuteron are frequently chosen as reference nuclei in the R_{F_2} quantity:

$$R_{F_2}^A = \frac{A^{\rm ref} F_2^A}{A F_2^{A^{\rm ref}}}. \tag{12}$$

In Fig. 4, we have calculated the R ratio for different targets at $x < 0.1$ by taking *deuterons* [Figs. 4(a)–4(c)] and

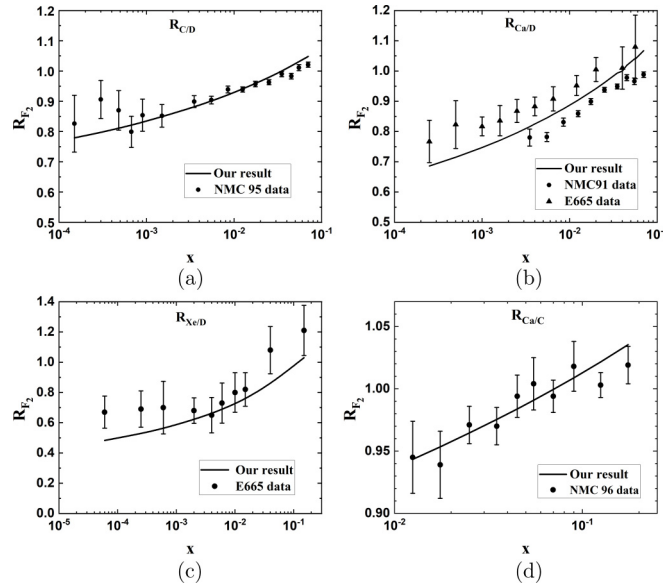

FIG. 4. R_{F_2} vs x. The nuclear target is determined in each frame.

carbon [Fig. 4(d)] as reference nuclei. The diagrams suggest the $R_{F_2}^A$ values rise by increasing x. In Fig. 4, data of the NMC and E665 Collaborations have Q^2 values between 0.5 and 26 GeV^2 and 0.01 and 22.5 GeV^2, respectively. This experimental range is between 3.4 and 35.3 GeV^2 for Fig. 4(d).

In Fig. 5, we expanded our study on the R_{F_2} ratio at low x. Having a glance at Fig. 5(a), we can conclude that heavier nuclei take lower values of R_{F_2} at definite Q^2. The effect of Q^2 on R is considered in Fig. 5(b). It shows that R is increased with Q^2, but the different choices of Q^2 change R insignificantly for a definite nucleus at low x. We note that it is reasonable as the result of geometric scaling explained in the Introduction. It means that Q^2 dependency by itself cannot control the cross section at small x. The line of $Q^2 = 10$ GeV^2 is higher than that of $Q^2 = 1.69$ GeV^2, although they come closer together at very low x ($x < 10^{-4}$).

Finally, we have compared our analysis with the other models in Fig. 6 for the moderate, high, and low ranges of Q^2. In Fig. 6(a), the result of our calculation for $R_{F_{\rm Fe/D}}$ at $Q^2 = 20$ GeV^2 is compared with experimental fitted parametrization models of nCTEQ15 [66] (solid lines), HKN [67] (dashed line), and EPS [68] (dotted line). These articles give a global

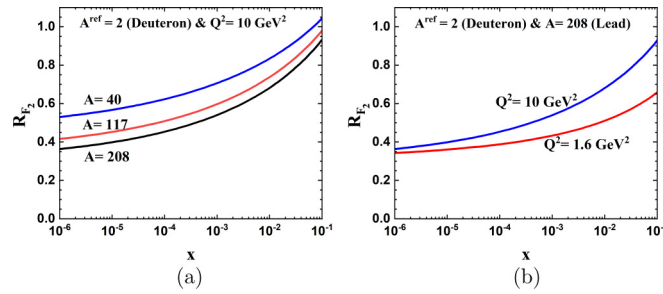

FIG. 5. R_{F_2} versus x. Investigating the effect of atomic mass corresponding to calcium, tin, and lead nuclei (a) and the effect of Q^2 (b).

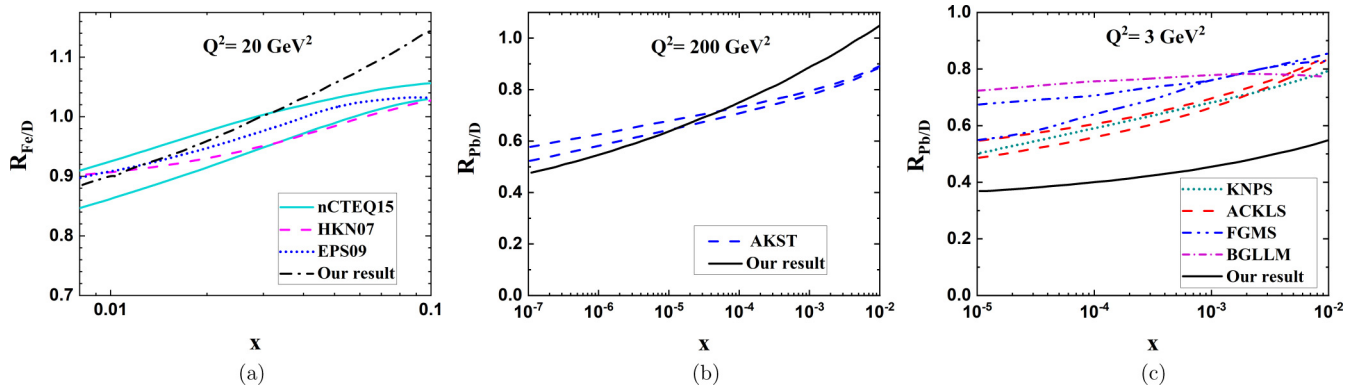

FIG. 6. Predictions of different models for R_{F_2} versus x. Our result for $R_{\mathrm{Fe/D}}$ is compared to the nCTEQ15, HKN07, and EPS09 phenomenological models (a). We have compared our result for $R_{\mathrm{Pb/D}}$ with AKST in panel (b) and with KNPS, ACKLS, FGMS, and BGLLM in panel (c).

analysis of nPDFs at next to leading order using the features of the QCD improved parton model and the χ^2 analyses as a statistical tool to improve accuracy. We should emphasize that the beginning of the shadowing effect is intended here; therefore, we have considered the domain of $8 \times 10^{-3} < x < 0.1$ in this diagram. Comparing them, we can see that our analysis coincides with these fitted models, especially at low x.

Figures 6(b) and 6(c) show the $R_{\mathrm{Pb/D}}$ versus x for $Q^2 = 200$ and 3 GeV^2, respectively. We have presented the comparison of our result with some theoretical and phenomenological models, such as AKST [69], KNPS [70], ACKLS [71], FGMS [72], and BGLLM [73].

In Fig. 6(b), it can be seen that our results are in agreement with those of other analyses. AKST has used a model based on the expansion of $\gamma^* A$ cross sections in multiple scattering series by considering two unitarization schemes tagged with Schwimmer and eikonal models.

Figure 6(c) indicates that our model takes a lower $R_{\mathrm{Pb/D}}$ for small Q^2. This difference becomes negligible in the low-x region.

In Fig. 6(c), one of the models we have compared our result with is KNPS [70], in which a numerical analysis is carried out to study nuclear shadowing in DIS off nuclei using the Green's function approach and dipole picture. This model is limited to low Q^2 and $x \leqslant 0.1$ where the antishadowing effect is omitted. Our computation is restricted to low x as well. Another phenomenological model which we used to make a comparison is that of Frankfurt *et al.* (FGMS) [72]. The authors of this article consider two different parametrizations of PDFs to investigate the leading twist approach to nuclear shadowing numerically. Armesto *et al.* [71] has studied nuclear structure functions in the $x \leqslant 0.01$ and $Q^2 \leqslant 10$ GeV^2 region using the relation between diffractive cross section measured in DIS on nucleons and nuclear shadowing based on the reggeon calculus. The last model shown in Fig. 6(c) is that of Bartels *et al.* (BGLLM) [73]. They have presented photoproduction cross sections assuming the QCD saturation effect and have used a dipole cross section by solving the BK evolution equation approximately.

Looking at these different models and predictions in various regions of x and Q^2, we note that more precise experimental data is required.

IV. CONCLUSIONS AND SUMMARY

In this paper, we presented a dipole cross section of Eq. (11) based on the KLN assumption about the gluon structure function of a proton. In this way, we get a total nuclear cross section that supports all nuclei targets in the color dipole picture that is valid for the region of $x \leqslant 10^{-2}$, so it does not include the antishadowing effect.

Starting with a hydrogen target and considering just the light quark masses, we expanded our calculation to other nuclei by studying their total cross sections, structure functions, R_{F_2} ratios, and shadowing and saturation effects in DIS off nuclei. We found a good agreement between our analysis and HERA, CERN and FermiLab data by comparing our results with existing experimental data.

As our important conclusion, we believe that the small-x saturation is more visible in heavier nuclei collisions [Figs. 5(a) and Fig. 4]. Besides that, the KLN model could be a reliable method that could be expanded more to get a better precision. Only a small number of experimental parameters are determined in our analysis, which makes it a simpler, but effective, method. As another conclusion, we think that, in a very-small-x region, the R_{F_2} ratio for a definite nucleus and different values of Q^2 are very close to each other [Fig. 5(b)]. This means that Q^2 dependency is not the only effective variable in describing total cross sections in an extra-small-x region.

We are investigating diffractive dissociation by applying our calculations on this process in electron-nucleus collisions for our next work.

[1] A. M. Cooper-Sarkar, R. C. E. Devenish, and A. De Roeck, Structure functions of the nucleon and their interpretation, Int. J. Mod. Phys. A **13**, 3385 (1998).

[2] S. Forte, Structure functions and parton distributions, Nucl. Phys. A **755**, 100 (2005).

[3] A. Accardi *et al.*, Electron ion collider: The next QCD frontier: Understanding the glue that binds us all, Eur. Phys. J. A **52**, 268 (2016).

[4] E. C. Aschenauer, S. Fazio, J. H. Lee, H. Mantysaari, B. S. Page, B. Schenke, T. Ullrich, R. Venugopalan, and P. Zurita, The electron-ion collider: Assessing the energy dependence of key measurements, Rep. Prog. Phys. **82**, 024301 (2019).

[5] P. Agostini *et al.* (LHeC Collaboration and FCC-he Study Group), The large hadron-electron collider at the HL-LHC, J. Phys. G: Nucl. Part. Phys. **48**, 110501 (2021).

[6] L. N. Lipatov, Reggeization of the vector meson and the vacuum singularity in nonabelian gauge theories, Sov. J. Nucl. Phys. **23**, 338 (1976).

[7] E. A. Kuraev, L. N. Lipatov, and V. S. Fadin, The Pomeranchuk singularity in nonabelian gauge theories, Sov. Phys. JETP **45**, 199 (1977).

[8] I. I. Balitsky and L. N. Lipatov, The Pomeranchuk singularity in quantum chromodynamics, Sov. J. Nucl. Phys. **28**, 822 (1978).

[9] L. V. Gribov, E. M. Levin, and M. G. Ryskin, Semihard processes in QCD, Phys. Rep. **100**, 1 (1983).

[10] I. Balitsky, Operator expansion for high-energy scattering, Nucl. Phys. B **463**, 99 (1996).

[11] Y. V. Kovchegov, Small-xF_2 structure function of a nucleus including multiple pomeron exchanges, Phys. Rev. D **60**, 034008 (1999).

[12] Y. V. Kovchegov, Introduction to the physics of saturation, Nucl. Phys. A **854**, 3 (2011).

[13] A. Deur, S. J. Brodsky, and G. F. de Teramond, The QCD running coupling, Prog. Part. Nucl. Phys. **90**, 1 (2016).

[14] A. L. Ayala, M. B. Gay Ducati, and E. M. Levin, QCD evolution of the gluon density in a nucleus, Nucl. Phys. B **493**, 305 (1997).

[15] D. Kharzeev, E. Levin, and M. Nardi, QCD saturation and deuteron nucleus collisions, Nucl. Phys. A **730**, 448 (2004).

[16] F. Carvalho, F. O. Duraes, S. Szpigel, and F. S. Navarra, Phenomenological tests of the Kharzeev-Levin-Nardi model, Nucl. Phys. B Proc. Suppl. **199**, 141 (2010).

[17] Z. Jalilian and G. R. Boroun, The universal function in color dipole model, Phys. Lett. B **773**, 455 (2017).

[18] G. R. Boroun, B. Rezaei, and S. Heidari, Nuclear longitudinal structure function in *eA* processes at the LHeC, Int. J. Mod. Phys. A **32**, 1750197 (2017).

[19] M. Wüsthoff and A. D. Martin, The QCD description of diffractive processes, J. Phys. G: Nucl. Part. Phys. **25**, R309 (1999).

[20] V. Barone and E. Predazzi, *High-Energy Particle Diffraction*, Texts and Monographs in Physics (Springer-Verlag, Berlin, 2002) Vol. 565.

[21] N. N. Nikolaev and B. G. Zakharov, Color transparency and scaling properties of nuclear shadowing in deep inelastic scattering, Z. Phys. C: Part. Fields **49**, 607 (1991).

[22] J. J. Ethier and E. R. Nocera, Parton distributions in nucleons and nuclei, Annu. Rev. Nucl. Part. Sci. **70**, 43 (2020).

[23] G. R. Boroun and B. Rezaei, The study of the gluon distribution function and reduced cross section behavior using the proton structure function, Nucl. Phys. A **1006**, 122062 (2021).

[24] G. R. Boroun and S. Zarrin, An approximate approach to the nonlinear DGLAP evaluation equation, Eur. Phys. J. Plus **128**, 119 (2013).

[25] K. J. Golec-Biernat and M. Wüsthoff, Saturation effects in deep inelastic scattering at low Q^2 and its implications on diffraction, Phys. Rev. D **59**, 014017 (1998).

[26] A. M. Stasto, K. J. Golec-Biernat, and J. Kwiecinski, Geometric Scaling for the Total $\gamma^* p$ Cross-Section in the Low x Region, Phys. Rev. Lett. **86**, 596 (2001).

[27] E. Iancu, A. Leonidov, and L. McLerran, The colour glass condensate: An introduction, in *QCD Perspectives on Hot and Dense Matter* (Springer Netherlands, Dordrecht, 2002), pp. 73–145.

[28] L. D. McLerran, *The color glass condensate and small x physics: Four lectures, in Lectures on Quark Matter*, Lecture Notes in Physics (Springer, Berlin, 2002) Vol. 583, p. 291.

[29] F. Gelis, E. Iancu, J. Jalilian-Marian, and R. Venugopalan, The color glass condensate, Annu. Rev. Nucl. Part. Sci. **60**, 463 (2010).

[30] N. Armesto, Introduction to low x physics and saturation, Acta Phys. Polon. B **35**, 213 (2004).

[31] E. Iancu, K. Itakura, and L. McLerran, Geometric scaling above the saturation scale, Nucl. Phys. A **708**, 327 (2002).

[32] G. R. Boroun and B. Rezaei, Geometrical scaling in charm structure function ratios, Nucl. Phys. A **929**, 119 (2014).

[33] G. R. Boroun, Color dipole cross section in the DGLAP improved saturation model, arXiv:2205.04889 [Eur. Phys. J. C (to be published 2022)].

[34] V. P. Goncalves and M. V. T. Machado, Geometric Scaling in Inclusive Charm Production, Phys. Rev. Lett. **91**, 202002 (2003).

[35] G. R. Boroun, Geometrical scaling of heavy-quark contributions in the low x region, arXiv:2204.07981.

[36] G. Watt and H. Kowalski, Impact parameter dependent color glass condensate dipole model, Phys. Rev. D **78**, 014016 (2008).

[37] H. Kowalski and D. Teaney, Impact parameter dipole saturation model, Phys. Rev. D **68**, 114005 (2003).

[38] A. H. Rezaeian and I. Schmidt, Impact-parameter dependent color glass condensate dipole model and new combined HERA data, Phys. Rev. D **88**, 074016 (2013).

[39] J. L. Albacete, N. Armesto, J. G. Milhano, and C. A. Salgado, Nonlinear QCD meets data: A global analysis of lepton-proton scattering with running coupling Balitsky-Kovchegov evolution, Phys. Rev. D **80**, 034031 (2009).

[40] N. Armesto, A Simple model for nuclear structure functions at small x in the dipole picture, Eur. Phys. J. C **26**, 35 (2002).

[41] K. V. Shajesh, The eikonal approximation, in *An Introduction to Inverse Problems in Physics* (World Scientific, Singapore, 2020), Chap. 10, pp. 195–205.

[42] R. J. Glauber, Cross sections in deuterium at high energies, Phys. Rev. **100**, 242 (1955).

[43] V. P. Gonçalves, G. Sampaio dos Santos, and C. R. Sena, Probing the saturation effects in the inclusives observables at the future *ep*/*eA* collider at the LHC, Nucl. Phys. A **978**, 187 (2018).

[44] M. Arneodo, Nuclear effects in structure functions, Phys. Rep. **240**, 301 (1994).

[45] S. Heidari, B. Rezaei, and G. R. Boroun, The study of deep inelastic scattering process of electron nucleus at LHeC region, Int. J. Mod. Phys. E **26**, 1750067 (2017).

[46] N. Nikolaev and B. Zakharov, Scaling properties of nuclear shadowing in deep inelastic scattering, Phys. Lett. B **260**, 414 (1991).

[47] N. Nikolaev and B. G. Zakharov, Pomeron structure function and diffraction dissociation of virtual photons

in perturbative QCD, Z. Phys. C: Part. Fields **53**, 331 (1992).
[48] V. Barone, M. Genovese, N. N. Nikolaev, E. Predazzi, and B. Zakharov, Nucleon sea parton densities: Differences for neutrinos and muons, Phys. Lett. B **268**, 279 (1991).
[49] N. N. Nikolaev and B. G. Zakharov, On determination of the large 1/x gluon distribution at HERA, Phys. Lett. B **332**, 184 (1994).
[50] M. Glück, E. Reya, and A. Vogt, Dynamical parton distributions revisited, Eur. Phys. J. C **5**, 461 (1998).
[51] K. Golec-Biernat and S. Sapeta, Saturation model of DIS: An update, J. High Energy Phys. **2018**, 102 (2018).
[52] S. Aid *et al.* (H1 Collaboration), A Measurement and QCD analysis of the proton structure function F_2 (x, Q^2) at HERA, Nucl. Phys. B **470**, 3 (1996).
[53] C. Adloff *et al.* (H1 Collaboration), A Measurement of the proton structure function $F_2(x, Q^2)$ at low x and low Q^2 at HERA, Nucl. Phys. B **497**, 3 (1997).
[54] J. Breitweg *et al.* (ZEUS Collaboration), Measurement of the proton structure function F_2 and ${\sigma_{\rm tot}}^{\gamma^* \rm p}$ at low Q^2 and very low x at HERA, Phys. Lett. B **407**, 432 (1997).
[55] F. D. Aaron *et al.* (H1 and ZEUS Collaborations), Combined measurement and QCD analysis of the inclusive $e^{\pm}p$ scattering cross sections at HERA, J. High Energy Phys. **2010**, 109 (2010).
[56] F. D. Aaron *et al.* (H1 Collaboration), A precision measurement of the inclusive ep scattering cross section at HERA, Eur. Phys. J. C **64**, 561 (2009).
[57] C. Ewerz, A. von Manteuffel, O. Nachtmann, and A. Schoning, The new F_L measurement from HERA and the dipole model, Phys. Lett. B **720**, 181 (2013).
[58] V. Andreev *et al.* (H1 Collaboration), Measurement of inclusive ep cross sections at high Q^2 at $\sqrt{s} = 225$ and 252 GeV and of the longitudinal proton structure function F_L at HERA, Eur. Phys. J. C **74**, 2814 (2014).
[59] P. Amaudruz *et al.* (New Muon Collaboration), A re-evaluation of the nuclear structure function ratios for D, He, ^{6}Li, C and Ca, Nucl. Phys. B **441**, 3 (1995).
[60] M. Arneodo *et al.* (New Muon Collaboration), The structure function ratios $F_2^{\rm Li}/F_2^D$ and F_2^C/F_2^D at small x, Nucl. Phys. B **441**, 12 (1995).
[61] M. Arneodo *et al.* (New Muon Collaboration), The A dependence of the nuclear structure function ratios, Nucl. Phys. B **481**, 3 (1996).
[62] M. Arneodo *et al.* (New Muon Collaboration), The Q^2 dependence of the structure function ratio $F_2^{\rm Sn}/F_2^{\rm C}$ and the difference $R^{\rm Sn} - R^{\rm C}$ in deep inelastic muon scattering, Nucl. Phys. B **481**, 23 (1996).
[63] P. Amaudruz *et al.* (New Muon Collaboration), Precision measurement of the structure function ratios $F_2^{\rm He}/F_2^{\rm D}$, $F_2^{\rm C}/F_2^{\rm D}$ and $F_2^{\rm Ca}/F_2^{\rm D}$, Z. Phys. C: Part. Fields **51**, 387 (1991).
[64] M. R. Adams *et al.* (E665 Collaboration), Saturation of Shadowing at Very Low Bjorken x, Phys. Rev. Lett. **68**, 3266 (1992).
[65] M. R. Adams *et al.* (E665 Collaboration), Shadowing in inelastic scattering of muons on carbon, calcium and lead at low $x_{\rm Bj}$, Z. Phys. C: Part. Fields **67**, 403 (1995).
[66] K. Kovařík *et al.*, nCTEQ15: Global analysis of nuclear parton distributions with uncertainties in the CTEQ framework, Phys. Rev. D **93**, 085037 (2016).
[67] M. Hirai, S. Kumano, and T. H. Nagai, Determination of nuclear parton distribution functions and their uncertainties in next-to-leading order, Phys. Rev. C **76**, 065207 (2007).
[68] K. J. Eskola, H. Paukkunen, and C. A. Salgado, EPS09: A new generation of NLO and LO nuclear parton distribution functions, J. High Energy Phys. **2009**, 065 (2009).
[69] N. Armesto, A. B. Kaidalov, C. A. Salgado, and K. Tywoniuk, Nuclear shadowing in Glauber-Gribov theory with Q^2-evolution, Eur. Phys. J. C **68**, 447 (2010).
[70] B. Z. Kopeliovich, J. Nemchik, I. K. Potashnikova, and I. Schmidt, Gluon shadowing in DIS off nuclei, J. Phys. G: Nucl. Part. Phys. **35**, 115010 (2008).
[71] N. Armesto, A. Capella, A. B. Kaidalov, J. Lopez-Albacete, and C. A. Salgado, Nuclear structure functions at small x from inelastic shadowing and diffraction, Eur. Phys. J. C **29**, 531 (2003).
[72] L. Frankfurt, V. Guzey, M. McDermott, and M. Strikman, Nuclear shadowing in deep inelastic scattering on nuclei: Leading twist versus eikonal approaches, J. High Energy Phys. **2002**, 027 (2002).
[73] J. Bartels, E. Gotsman, E. Levin, M. Lublinsky, and U. Maor, QCD saturation and photoproduction on proton and nuclei targets, Phys. Rev. D **68**, 054008 (2003).